Chemical Science

EDGE ARTICLE

View Article Online
View Journal | View Issue

Cite this: *Chem. Sci.*, 2019, **10**, 1368

All publication charges for this article have been paid for by the Royal Society of Chemistry

Oxygen uptake in complexes related to [NiFeS]- and [NiFeSe]-hydrogenase active sites†

Xuemei Yang, Lindy C. Elrod, Joseph H. Reibenspies, Michael B. Hall* and Marcetta Y. Darensbourg *

A biomimetic study for S/Se oxygenation in Ni(μ-EPh)(μ-SN_2)Fe, (E = S or Se; SN_2 = Me-diazacycloheptane-CH_2CH_2S); Fe = (η^5-C_5H_5)Fe^{II}(CO) complexes related to the oxygen-damaged active sites of [NiFeS]/[NiFeSe]-H_2ases is described. Mono- and di-oxygenates (major and minor species, respectively) of the chalcogens result from exposure of the heterobimetallics to O_2; one was isolated and structurally characterized to have Ni–O–Se_{Ph}–Fe–S connectivity within a 5-membered ring. A compositionally analogous mono-oxy species was implicated by ν(CO) IR spectroscopy to be the corresponding Ni–O–S_{Ph}–Fe–S complex; treatment with O-abstraction agents such as P(*o*-tolyl)$_3$ or PMe_3 remediated the O damage. Computational studies (DFT) found that the lowest energy isomers of mono-oxygen derivatives of Ni(μ-EPh)(μ-SN_2)Fe complexes were those with O attachment to Ni rather than Fe, a result consonant with experimental findings, but at odds with oxygenates found in oxygen-damaged [NiFeS]/[NiFeSe]-H_2ase structures. A computer-generated model based on substituting $^-$SMe for the N-$CH_2CH_2S^-$ sulfur donor of the N_2S suggested that constraint within the chelate hindered O-atom uptake at that sulfur site.

Received 5th October 2018
Accepted 4th November 2018

DOI: 10.1039/c8sc04436h

rsc.li/chemical-science

Introduction

Hydrogenases are metalloenzymes that catalyze reversible H_2 production from protons and electrons. Likely originating in pre-biotic ages and under a reducing atmosphere, the active sites contain iron, nickel and sulfur, along with simple diatomic ligands, CO and CN, in optimal arrangements that produce superb biocatalysts found throughout nature.[1] These structures offer guidance for design of molecular catalysts comprising earth abundant metals for application in electrolyzers and fuel cells.[2,3] While the protein superstructures protect the biological redox centers from O_2 as an oxidant that competes with protons, there is ample evidence, including protein crystal structures, of the detrimental effects of O_2 invasion into the active site. Indeed the initial understanding of the [NiFeS]-H_2ase was plagued with Ni-based EPR signals from various deactivated enzyme states damaged by partial oxidation or oxygenation. Vague terms such as "ready" and "unready" states, with recovery from oxygen damage on the order of seconds *vs.* hours, respectively, were adopted in attempts to express reductive (added H_2 or $H^+ + e^-$) reactivation requirements.[4,5]

As shown in Fig. 1 two subclasses exist for the [NiFe]-H_2ase enzymes. The predominant form, [NiFeS]-H_2ase, contains a set of four cysteines around Ni; two Cys-S bridge Ni to an $Fe^{II}(CO)(CN)_2$ unit. A second form, [NiFeSe]-H_2ase is identical to the [NiFeS]-H_2ase except a terminal cysteine is replaced by selenocysteine. As the incorporation of selenocysteine requires an intricate dedicated biosynthetic machinery, as well as a high energetic cost, this form is found in few microorganisms; an example is *Methanococcus voltae*.[6,7]

Despite sharing similar active site structures, [NiFeSe]-H_2ase is deemed superior to the all-sulfur, [NiFeS]-H_2ase, with respect to H_2 production and O_2 tolerance, the latter defined as resistance to O_2 and recovery of full activity on appropriate reductive treatment.[4,8,9] Fundamental differences between sulfur and selenium include the higher acidity of Se-Cys, which might account for the proton reduction disparities, while the low redox potential and high nucleophilicity of selenium in selenolates relative to sulfur in thiolates might account for the higher oxygen-tolerance of [NiFeSe]-H_2ase.[7]

Both the ready and unready states of [NiFeS]-H_2ase are identified as containing Ni^{III}; the ready state contains a hydroxide bridge between Ni and Fe, (Ni–**B**), while the unready state is proposed to contain a κ_1-peroxide bridge or a sulfenate within a 5-membered Ni–O–S_{cys}–Fe–S_{cys} ring (Ni–**A**), as depicted in Fig. 1.[10,11] However, in [NiFeSe]-H_2ase, there are thus far revealed only rapid recovery or ready states comprised of oxygenates of Se- and S-cysteines; selected structures are shown in Fig. 1.[9] Notably, multiple levels of oxidized chalcogenide sites, both S and Se, have been uncovered in [NiFeSe]-H_2ase; nevertheless the basic NiFe core structure is maintained and reductive repair is possible. As these oxygenated chalcogenides play vital roles in the reversibility of oxygen damage, small

Texas A&M University, Department of Chemistry, College Station, TX 77843, USA. E-mail: marcetta@chem.tamu.edu

† Electronic supplementary information (ESI) available. CCDC 1861574, 1861577–1861580 and 1861890. For ESI and crystallographic data in CIF or other electronic format see DOI: 10.1039/c8sc04436h

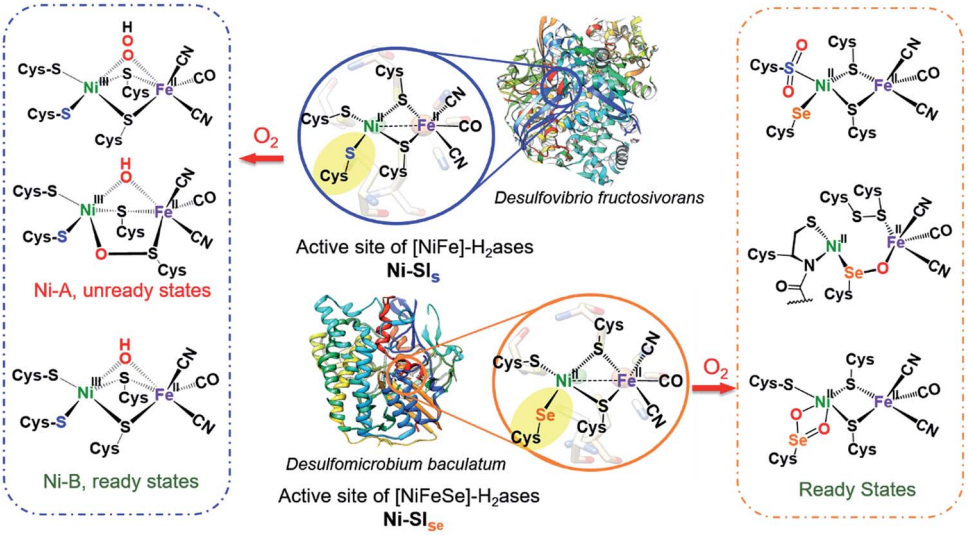

Fig. 1 Reduced (middle) active sites of [NiFe]-H_2ases and selected oxidized active sites of [NiFeS] (left) and [NiFeSe]-H_2ases (right).[8,9,15,16]

molecule analogues are needed to explore aerobic damage and repair, both for insight into the enzyme as well as the design of robust synthetic catalysts. Examples are limited.

Ogo, *et al.* isolated a high valent iron(IV) peroxo complex on reacting solvent-coordinated complexes $[Ni^{II}LFe^{II}(RCN)(\eta^5\text{-}C_5Me_5)]^+$ with O_2.[12–14] However, no oxygenated sulfur species were reported from their system. The first S-oxygenated [NiFe] complex was reported by Driess's lab as a model for sulfenate intermediates in O_2-tolerant hydrogenase; it was synthesized from $FeBr_2$ and the pre-formed sulfenato nickel complex[17] rather than direct oxygenation.[18]

Herein, we describe a biomimetic study for S/Se oxygenation in complexes Ni(μ-EPh)(μ-SR′)Fe, (E = S or Se; R′ = N_2S) with certain features of the [NiFeS]/[NiFeSe]-H_2ases' active sites. We report the first XRD structure of an oxygenate of selenium within a Ni–Fe complex and use it as a reference point for DFT computational analyses and predictions.

Results and discussion

Synthesis and characterizations

Nickel dithiolate complexes such as NiN_2S_2 are well known to react as metalloligands by formation of Ni-$(\mu_2\text{-SR})_2$-M′ bridges.[19] Adopting a $[NiN_2S]_2^{2+}$ bimetallic nickel dimer[20] as platform for dimer cleavage reactions,[19,21,22] we have derived monomeric $Ni(N_2S)(EPh)$ (E = S and Se, complexes **A** and **B**, respectively). These *cis*-dichalcogenides are subsequently used as metalloligands to an iron receiver unit, $(\eta^5\text{-}C_5H_5)Fe^{II}(CO)^+$, in analogy to well-known NiN_2S_2 derivatives.[23] The synthetic scheme shown in Fig. 2 is further detailed (mass spectra, elemental analyses, ^1H and ^{13}C NMR spectra, and XRD crystal structures) in the ESI.† The lower value of ν(CO) (1934 cm^{-1}) in the $NiSe_{Ph}Fe^+$, complex **2**, as contrasted to $NiS_{Ph}Fe^+$, complex **1** (1939 cm^{-1}), is attributed to the better electron donor properties of Se over S,[7] resulting in better pi-backbonding from Fe^{II} to the CO reporter ligand.

X-ray quality crystals of monomeric Ni complex **A** were obtained by diethyl ether vapor transfer into a solution of CH_3CN. Complex **B** and the Ni–Fe complexes (**1**, **2** and **2′**), were crystallized from a pentane-layered CH_2Cl_2 solution at −35 °C. Polymorphs, **2** and **2′**, are distinguished by the orientation of the SePh planes in the $NiSe_{Ph}Fe^+$ complexes. Dark red needle crystals of **2** exist in a pbca space group; **2′**, as dark red blocks, is in the $P2_1/c$ space group.

Molecular structures determined by XRD are unexceptional, Fig. 3. The >3.0 Å distances between Ni and Fe are beyond bonding. The $NiE_{Ph}Fe^+$ complex structures find a typical piano-stool geometry exists about the $[(\eta^5\text{-}C_5H_5)Fe(CO)]^+$ unit, and, as usual for bridging dithiolates, butterfly-like cores are due to the lone pair-imposed steric requirement of the chalcogenide

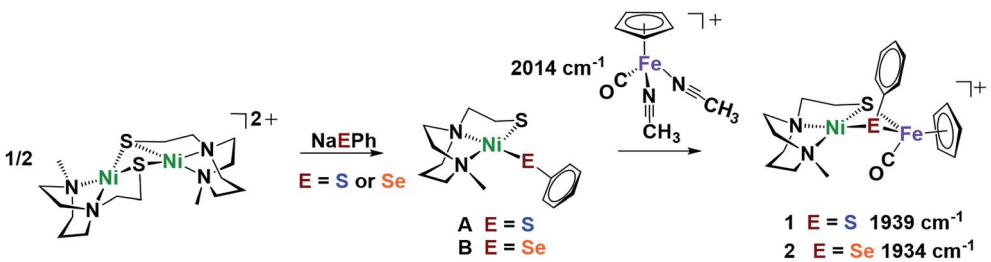

Fig. 2 Synthetic scheme for $NiE_{Ph}Fe^+$ complexes **1** and **2**. The ν(CO) IR values of the products recorded in CH_2Cl_2.

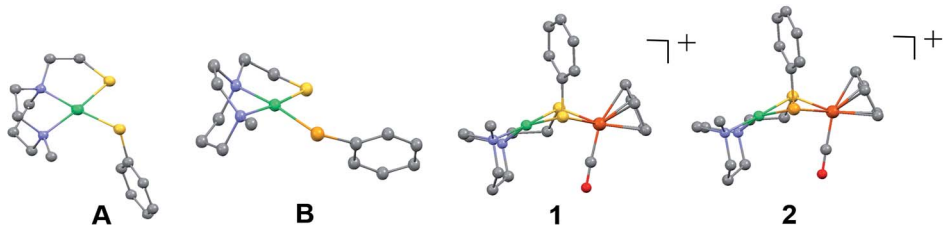

	A	B	1	2
Ni···Fe/Å	-	-	3.170	3.253
Ni-E_{Ar}/Å	2.184(3)	2.309(6)	2.199(1)	2.311(1)
Fe-E_{Ar}/Å	-	-	2.300(2)	2.406(1)
∠Fe-E_{Ar}-Ni/°	-	-	89.57(5)	87.17(4)
∠S-Fe-E_{Ar}/°	-	-	79.40(5)	79.62(5)
∠S-Ni-E_{Ar}/°	88.4(3)	94.19(3)	84.71(5)	84.47(6)
∠E_{Ar}-Ni-N	100.3(3)	93.94(8)	101.1(1)	101.4(2)
E_{Ar}-C_{Ph}	1.754(6)	1.918(3)	1.789(5)	1.931(6)
Hinge angle/°	-	-	141.15	142.69

Fig. 3 Molecular structures of **A**, **B** and **1** ($NiS_{Ph}Fe$), **2** ($NiSe_{Ph}Fe$), determined by single-crystal XRD, with the BF_4^- ions and H atoms omitted. E in **A** and **1** is sulfur; E in **B** and **2** is selenium.

bridges. Hinge angles, defined as the intersection of the best N_2SE plane with the SEFe plane, are *ca.* 140–145°. The selenium-containing complexes, **2** and **2′** contain hinge angles slightly larger than found in **1**.

Reactivity

The chemical responsiveness of the heterobimetallic complexes was illustrated by reaction with CO(g) which, in both the $NiS_{Ph}Fe^+$ and $NiSe_{Ph}Fe^+$ complexes, resulted in Ni–Fe splitting by transferring the EPh to Fe, generating $(\eta^5\text{-}C_5H_5)Fe(CO)_2EPh$, and returned the Ni to its $[NiN_2S]_2^{2+}$ dimeric form. On mixing complex **1** with an excess of Na^+SePh^- in 5 : 1 CH_2Cl_2/MeOH, complex **2** is formed over the course of hours. The opposite, *i.e.*, an attempt to replace the bridging $SePh^-$ in complex **2** by SPh^-, was unsuccessful. These reactions emphasize the mobility of the EPh^- unit in the $NiE_{Ph}Fe^+$ complex.

At 22 °C, O_2 gas was bubbled through CH_2Cl_2 solutions of heterobimetallic complexes **1** and **2**/**2′**; the reactions were monitored by FTIR spectroscopy. The clear reddish black solution of $NiSe_{Ph}Fe^+$ developed into a slightly cloudy, dark red solution after 2 h, with ν(CO) shifting from a sharp band at 1934 cm^{-1} to a broader band at 1954 cm^{-1}, designated as complex **2+O** (Fig. 4). On filtration, the mother liquor mainly contained complex **2+O** and, on removal of solvent and redissolving in CH_2Cl_2, a high resolution ESI-MS^+ showed the parent molecular ion to have *m*/*z* 552.9634 (calc. for $[\mathbf{2+O}]^+$, 552.9661). This mono-oxygenate was isolated in *ca.* 50% yield (Fig. S20†). The uptake of two oxygen atoms was additionally indicated by a minor signal at *m*/*z* 568.9419 (calc. for $[\mathbf{2+2O}]^+$, 568.9611). The

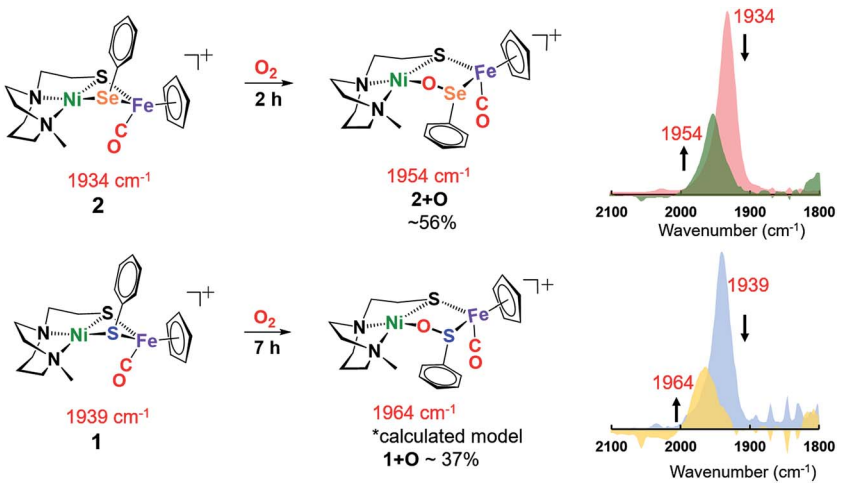

Fig. 4 Reactions of **1** and **2** in the presence of 1 atm O_2 in CH_2Cl_2 at 22 °C; conversions determined by ν(CO) analysis.

residue, which was soluble in CH_3CN, was confirmed as the $[NiN_2S]_2^{2+}$ dimer by XRD with crystals obtained by ether diffusion; it was isolated in 35% yield. A remaining insoluble yellow solid was found to be an iron(III) oxide complex (see ESI†). Reactions performed in air instead of pure O_2 yielded (more slowly) the same products.

The O_2-bubbled CH_2Cl_2 solution of the all-sulfur analogue $NiS_{Ph}Fe^+$, **1**, required 7 h to completion, indicated by the decrease in IR absorption at ν(CO) 1939 cm^{-1} as the oxidized species appeared as a broad band at ν(CO) 1964 cm^{-1} (Fig. 4). The reactivity (time) difference is consistent with the fact that S^{2-} is oxidized with more difficulty than Se^{2-}.[7] The high resolution ESI-MS^+ of products from **1** and O_2 in CH_3CN indicated the uptake of one, two, and three oxygens (Fig. S19†). Based on DFT calculations (*vide infra*), complex **1+O** is of a similar structure as **2+O**. Both **1+O** and **2+O** show sharp signals in their NMR spectra and are EPR-silent, indicating that Ni and Fe are low spin, +2 species (Fig. S30, S31 and S38†). To confirm that the **1+O** and **2+O** were derived from molecular O_2, the same reactions were carried out with added $^{18}O_2$. Mass spectral analysis indicated the uptake of labelled O-18, Fig. S43 and S44.†

Crystals of complex **2+O** were obtained by layering pentane on DCM solutions of **2+O**. As seen in Fig. 5, complex **2+O** contains a 5-membered, puckered NiOSeFeS ring; the Ni(II) is the center of a square planar N_2SO binding site. From XRD the bond distances of Ni–S and Fe–S in **2+O** are largely the same as in the reduced form **2** (or **2′**); the oxygen insertion into the Ni–Se bond results in an Ni–O bond at 1.870(2) Å. The Fe–Se bond length becomes slightly shorter in **2+O**, 2.333(1) Å, as compared to **2**, 2.406(1) Å. The distance between Ni and Fe in **2+O** is 3.568 Å, *ca.* 0.3 Å longer than in the reduced form, reflecting the expansion of the ring. Note that the Ni–**A** form of the [NiFe]-H_2ase enzyme active site with sulfenate also has a 5-membered NiOSFeS ring, Fig. 1.[24] The Ni···O distance in Ni–**A** is 1.824 Å, while in **2+O** it is 1.870(2) Å. In contrast, a minor fraction from [NiFeSe]-H_2ase oxidation reported by Volbeda *et al.* has a different connectivity, NiSeOFe, Fig. 1.[9] Complex **2+O** is, to our knowledge, the first model of an oxygenated [NiFeSe]-H_2ase synthetic analogue derived from direct reaction.

As a comparison to the $NiE_{Ph}Fe$ complexes **1** and **2**, constrained NiN_2S_2 derivatives, $[NiN_2S_2{\cdot}Fe(\eta^5\text{-}C_5H_5)(CO)]^+[BF_4]^-$ and $[NiN_2S_2{\cdot}Fe(\eta^5\text{-}C_5Me_5)(CO)]^+[BF_4]^-$ N_2S_2 = bismercaptoethanediazacycloheptane) were tested for reactivity with oxygen.[25,26] After stirring their solutions in an O_2 atmosphere for several days, they remain intact with no indication of reaction. We surmise that the CO which is bound to Fe prevents O_2 activation at the Fe center and both sulfur and nickel are deactivated towards O_2 reactivity in the rigid chelating N_2S_2 ligands. However, in complexes **1** and **2**, the mobility at EPh (E = S or Se) provides a potential site for O_2 attack on the Ni or Fe, consistent with the splitting of **1** and **2** by CO(g) (Fig. S33†). For comparison, elevated temperature (70 °C) and 11 bar CO(g) are required to break one Ni–S bond in $[NiN_2S_2{\cdot}Fe(\eta^5\text{-}C_5H_5)(CO)]^+[BF_4]^-$.[25]

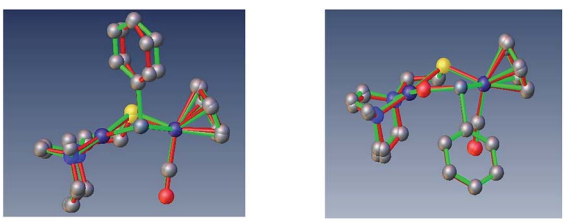

	2 Exp.	**2** Calc.		**2+O** Exp.	**2+O** Calc.
Ni- - -Fe/Å	3.253	3.23	Ni-Fe/Å	3.568	3.615
Ni-Se/Å	2.311(1)	2.338	Ni-Se/Å	3.168	3.209
Fe-Se/Å	2.406(1)	2.439	Ni-S/Å	2.153(1)	2.175
Ni-Se-Fe/°	87.17(4)	85.15	Ni-O/Å	1.870(2)	1.869
Hinge/°	142.69	136.77	Fe-S/Å	2.248(1)	2.280
			Fe-Se/Å	2.333(1)	2.336
			O-Ni-S/°	92.93(7)	93.05
			Se-Fe-S/°	86.15(3)	86.22

Fig. 5 Overlay of experimental and computational structures of **2** and **2+O** along with selected geometric parameters. Hydrogens deleted for clarity.

Computational section

The crystal structures of **2** and **2+O** were used as geometric starting points for DFT calculations (TPSSTPSS functional with the 6-311++G(d,p) basis set on all nonmetal atoms and the 6-311+G basis set for Ni and Fe atoms) and then optimized using the Gaussian 09 program using the SMD implicit solvation model with acetonitrile as the solvent.[28] Cartesian coordinates of calculated structures are given in the ESI.† The calculated structures for **2** and **2+O** showed excellent agreement with the corresponding experimental structures, Fig. 5. Similar structures were found for the sulfur analogues, **1** and **1+O**.

The structure of **2+O** was investigated to determine contributing factors to the thermodynamically favored oxygenation product. A less rigid model of **2+O** was made by breaking

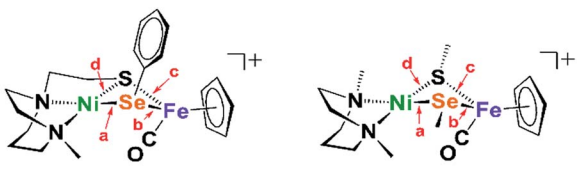

2+O **3+O**

	a	**b**	**c**	**d**
2+O	0	+8.6	+10.0	+15.5
3+O	+3.2	+10.0	+14.2	0

Fig. 6 Relative energies of oxygenated isomers of N_2SSe_{Ph} model, **2+O**, and the bidentate, separated donors in the $N_2S_{Me}Se_{Me}$ model, **3+O**, in kcal mol^{-1}. A range of functionals and basis sets were explored and found to elicit minor differences on energies of complexes but do not change the ordering of isomers' energies (Fig. S41†).

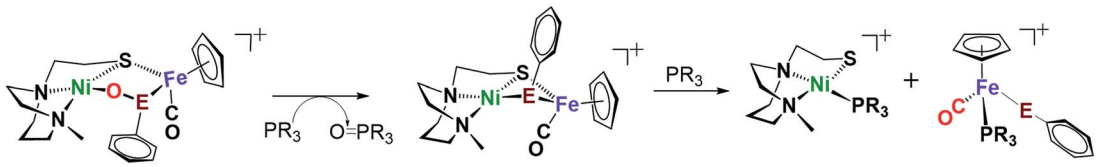

Fig. 7 Reaction of complex **2+O** (E = Se) or **1+O** (E = S) with O-abstracting agents, PR_3 (R = Me or *o*-tolyl).

the carbon–carbon bond linking the sulfur donor to the neighbouring nitrogen donor, changing the resulting methylene fragments into methyl groups, and replacing the phenyl group on Se-Ph with a methyl group. This bidentate $N_2S_{Me}Se_{Me}$ model, with unconnected SMe, is designated as **3** and is designed to create similar electronic, steric environments and constraints around the sulfur and selenium atoms.

Four oxygenated isomers, **3+O$_{a–d}$**, as well as four corresponding isomers, **2+O$_{a–d}$**, were calculated in which the location of the oxygen atom was varied according to the scheme described in Fig. 6. The isomer **2+O$_a$**, which corresponds to the experimental structure, is indeed the lowest energy isomer of **2+O**; the next lowest isomer, **2+O$_b$**, is 8.6 kcal higher in energy. This contrasts with the $N_2S_{Me}Se_{Me}$ model in which the lowest energy isomer, **3$_d$**, has the oxygen atom inserted between the nickel and the sulfur atoms rather than the nickel and selenium. The corresponding isomer **2+O$_d$** is the highest energy isomer for the tridentate model and the oxygen atom appears in a position bridging the nickel sulfur bond rather than full insertion. This is likely due to the geometric restraints imposed by the tridentate N_2S ligand that disfavor the addition of the oxygen atom into its rigid binding arrangement. This constraint is not found in the more open bidentate model with separated SMe donors. There it is found that formation of a sulfur–oxygen bond is thermodynamically favored, by 3.2 kcal mol^{-1}, as compared to the formation of a selenium–oxygen bond.

O-atom removal results

As arbiters between O_2 and the [NiFe] or [NiFeSe]-H_2ase active sites, chalcogenides prevent complete degradation of the organometallic active sites of hydrogenases, and perform this role reversably.[24,27] To explore the possibility of reversal of oxygenated selenate/sulfenate, O-abstracting agents, PR_3 (R = Me or *o*-tolyl), were employed for O-atom removal (Fig. 7). The ν(CO) monitor of the reaction of **2+O** and 1 equiv. of PMe_3 in DCM showed a band shift from 1954 to 1934 cm^{-1}. The latter absorption is made up from a mixture of complex **2** and the PMe_3 species $(\eta^5\text{-}C_5H_5)Fe(SePh)(PMe_3)(CO)$, which is confirmed by the $^+$ESI-MS data (Fig. S37†). The reaction of a mixture of **1+O** and **1+2O** with 1 equiv. of PMe_3 resulted in partial conversion of **1+O** to **1**, finding that **1+2O** was unchanged, even in presence of excess PMe_3. The $^+$ESI-MS (Fig. S36†) indicates the formation of reduced complex **2**, unreacted **1+2O** and the PMe_3 derivative $(\eta^5\text{-}C_5H_5)Fe(SPh)(PMe_3)(CO)$. Removal of the O-atom from **1+O** and **2+O** by reducing agents containing H^-, as well as electrochemically ($e^- + H^+$), have thus far been unsuccessful.

Conclusion

In summary, we have observed oxygenation and O-atom removal from two biomimetic complexes with features of the [NiFeS]/[NiFeSe]-H_2ase active sites. Our study highlights the usefulness of the $[NiN_2S]_2^{2+}$ synthetic platform for generating NiFe biomimetic complexes. Clearly the $NiE_{Ph}Fe^+$ complex differs from the active site of [NiFeSe]-H_2ase as the selenium in the model is in a bridging position, rather than terminal as nature has adopted. The relative reactivities however are consistent with what is found in nature. As compared to complex **1**, the selenium-bridged complex **2** required a shorter time to generate oxygenated selenium, **2+O**. The partial conversion of oxygenated chalcogenides (Se or S oxidation states of 0) back to reduced S/Se (oxidation state −2) in this study provides a foundation for the mechanism of reactivation of S/Se-oxygenated [NiFeE]-H_2ases. Oxygen-uptake by S/Se in [NiFeS]- and [NiFeSe]-H_2ases results in modification of the active site, but less severe than would result in irreparable degradation.[27] During the oxygenation and O-atom removal from the chalcogen atom, we note that the mobility in the Ni–E bond plays a vital role.

The variety of oxygenates thus far found in nature, Fig. 1, speak to the ability of the chalcogens to maintain a close attachment to the NiFe site. Detailed O_2/H_2ase active site reaction mechanisms remain obscure but of great interest.[29,30] Our studies of model complexes point to the possibility of opening the Ni–E bond in the Ni–(μE_{Ph})–Fe unit. Such bond cleavage exposes a reactive lone pair on sulfur or selenium that attracts the electrophilic O_2 molecule concomitant with providing an open site on Ni^{2+} for assisted activation, leading to the product. A related strategy for protection of the active site from oxidative damage is seen in the MBH (membrane-bound respiratory [NiFeS]-hydrogenase) wherein the proximal [4Fe-3S] cluster donates two electrons and one proton for reduction of adventitious O_2.[31]

Conflicts of interest

There are no conflicts to declare.

Acknowledgements

This work was funded by the National Science Foundation (CHE-1300787, CHE-1664866 to M. B. H. and CHE-1266097, CHE-1665258 to M. Y. D.) and the Robert A. Welch Foundation (A-0648 to M. B. H. and A-0924 to M. Y. D.).

Notes and references

1 W. Lubitz, H. Ogata, O. Rudiger and E. Reijerse, *Chem. Rev.*, 2014, **114**, 4081.
2 L. L. Beer, E. S. Boyd, J. W. Peters and M. C. Posewitz, *Curr. Opin. Biotechnol.*, 2009, **20**, 264.
3 M. Hambourger, M. Gervaldo, D. Svedruzic, P. W. King, D. Gust, M. Ghirardi, A. L. Moore and T. A. Moore, *J. Am. Chem. Soc.*, 2008, **130**, 2015.
4 C. S. A. Baltazar, M. C. Marques, C. M. Soares, A. M. DeLacey, I. A. C. Pereira and P. M. Matias, *Eur. J. Inorg. Chem.*, 2011, 948.
5 D. W. Wakerley and E. Reisner, *Energy Environ. Sci.*, 2015, **8**, 2283.
6 P. M. Vignais and B. Billoud, *Chem. Rev.*, 2007, **107**, 4206.
7 H. J. Reich and R. J. Hondal, *ACS Chem. Biol.*, 2016, **11**, 821.
8 M. C. Marques, R. Coelho, A. L. De Lacey, I. A. Pereira and P. M. Matias, *J. Mol. Biol.*, 2010, **396**, 893.
9 A. Volbeda, P. Amara, M. Iannello, A. L. De Lacey, C. Cavazza and J. C. Fontecilla-Camps, *Chem. Commun.*, 2013, **49**, 7061.
10 M. Horch, L. Lauterbach, M. A. Mroginski, P. Hildebrandt, O. Lenz and I. Zebger, *J. Am. Chem. Soc.*, 2015, **137**, 2555.
11 H. Ogata, W. Lubitz and Y. Higuchi, *Dalton Trans.*, 2009, 7577.
12 M. Isegawa, A. K. Sharma, S. Ogo and K. Morokuma, *Organometallics*, 2018, **37**, 1534.
13 T. Kishima, T. Matsumoto, H. Nakai, S. Hayami, T. Ohta and S. Ogo, *Angew. Chem., Int. Ed.*, 2016, **55**, 724.
14 T. Matsumoto, T. Kishima, T. Yatabe, K.-S. Yoon and S. Ogo, *Organometallics*, 2017, **36**, 3883.
15 E. Garcin, X. Vernede, E. Hatchikian, A. Volbeda, M. Frey and J. Fontecilla-Camps, *Structure*, 1999, **7**, 557.
16 A. Volbeda, M.-H. Charon, C. Piras, E. C. Hatchikian, M. Frey and J. C. Fontecilla-Camps, *Nature*, 1995, **373**, 580.
17 C. A. Grapperhaus and M. Y. Darensbourg, *Acc. Chem. Res.*, 1998, **31**, 451.
18 N. J. Lindenmaier, S. Wahlefeld, E. Bill, T. Szilvasi, C. Eberle, S. Yao, P. Hildebrandt, M. Horch, I. Zebger and M. Driess, *Angew. Chem., Int. Ed.*, 2017, **56**, 2208.
19 J. A. Denny and M. Y. Darensbourg, *Chem. Rev.*, 2015, **115**, 5248.
20 R. M. Jenkins, M. L. Singleton, L. A. Leamer, J. H. Reibenspies and M. Y. Darensbourg, *Inorg. Chem.*, 2010, **49**, 5503.
21 E. M. Gale, D. M. Cowart, R. A. Scott and T. C. Harrop, *Inorg. Chem.*, 2011, **50**, 10460.
22 D. Huang, L. Deng, J. Sun and R. H. Holm, *Inorg. Chem.*, 2009, **48**, 6159.
23 D. Brazzolotto, M. Gennari, N. Queyriaux, T. R. Simmons, J. Pecaut, S. Demeshko, F. Meyer, M. Orio, V. Artero and C. Duboc, *Nat. Chem.*, 2016, **8**, 1054.
24 A. Volbeda, L. Martin, E. Barbier, O. Gutiérrez-Sanz, A. L. D. Lacey, P.-P. Liebgott, S. b. Dementin, M. Rousset and J. C. Fontecilla-Camps, *J. Biol. Inorg Chem.*, 2014, **20**, 11.
25 S. Ding, P. Ghosh, A. M. Lunsford, N. Wang, N. Bhuvanesh, M. B. Hall and M. Y. Darensbourg, *J. Am. Chem. Soc.*, 2016, **138**, 12920.
26 P. Ghosh, M. Quiroz, N. Wang, N. Bhuvanesh and M. Y. Darensbourg, *Dalton Trans.*, 2017, **46**, 5617.
27 K. A. Vincent, A. Parkin, O. Lenz, S. P. J. Albracht, J. C. Fontecilla-Camps, R. Cammack, B. Friedrich and F. A. Armstrong, *J. Am. Chem. Soc.*, 2005, **127**, 18179.
28 M. J. Frisch; G. W. Trucks; H. B. Schlegel; G. E. Scuseria; M. A. Robb; J. R. Cheeseman; G. Scalmani;V. Barone; B. Mennucci; G. A. Petersson; H. Nakatsuji; M. Caricato; X. Li; H. P. Hratchian; A. F. Izmaylov; J. Bloino; G. Zheng; J. L. Sonnenberg; M. Hada; M. Ehara; K. Toyota; R. Fukuda; J. Hasegawa; M. Ishida; T. Nakajima; Y. Honda; O. Kitao; H. Nakai; T. Vreven; J. A. Montgomery Jr; J. E. Peralta; F. Ogliaro; M. Bearpark; J. J. Heyd; E. Brothers; K. N. Kudin; V. N. Staroverov; R. Kobayashi; J. Normand; K. Raghavachari; A. Rendell; J. C. Burant; S. S. Iyengar; J. Tomasi; M. Cossi; N. Rega; J. M. Millam; M. Klene; J. E. Knox; J. B. Cross; V. Bakken; C. Adamo; J. Jaramillo; R. Gomperts; R. E. Stratmann; O. Yazyev; A. J. Austin; R. Cammi; C. Pomelli; J. W. Ochterski; R. L. Martin; K. Morokuma; V. G. Zakrzewski; G. A. Voth; P. Salvador; J. J. Dannenberg; S. Dapprich; A. D. Daniels; O. Farkas; J. B. Foresman; J. V. Ortiz; J. Cioslowski; D. J. Fox, *Gaussian 09, revision D.01*, Gaussian, Inc., Wallingford, CT, 2009.
29 S. Ogo, *Coord. Chem. Rev.*, 2017, **334**, 43.
30 S. Ogo, *Chem. Rec.*, 2014, **14**, 397.
31 Y. Shomura, K. S. Yoon, H. Nishihara and Y. Higuchi, *Nature*, 2011, **479**, 253.